# Effect of core density on deformation and failure in sandwich composites subjected to underwater impulsive loads

by

**Siddharth Avachat and Min Zhou**

reprinted from

**THE INTERNATIONAL JOURNAL OF MULTIPHYSICS**

**2012: VOLUME 6 NUMBER 3**

**MULTI-SCIENCE PUBLISHING**

# Effect of core density on deformation and failure in sandwich composites subjected to underwater impulsive loads

**Siddharth Avachat and Min Zhou[1,*]**
The George W. Woodruff School of Mechanical Engineering,
The School of Materials Science and Engineering,
Georgia Institute of Technology,
Atlanta, GA 30332, USA

**ABSTRACT**

The response of sandwich structures to underwater blast loading is analyzed. The analysis focuses on the effect of varying structural attributes on energy dissipation and deformation. The structures analyzed are simply-supported sandwich structures with PVC foam cores and fiber-reinforced polymer composite facesheets. For the analysis carried out, the material properties of the sandwich cores are varied and the total mass is kept constant. In conjunction with experiments, simulations account for underwater blast loading on structures in air-backed and water-backed conditions. Core crushing is accounted for through the Deshpande and Fleck model and facesheet failure is accounted for using the Hashin damage model. Results reveal a significant difference between the response of air-backed and water-backed/submerged structures. In general, thick and low-density cores provide superior blast mitigation and failure resistance. Scaling relations are developed to quantify the responses. These relations can be used to optimize the design of sandwich structures in critical parts of ships like keel, turbine-blades and rudders which involve different contact conditions with water.

## 1. INTRODUCTION

Marine structures are designed to operate in hostile environments involving corrosive seawater, hot and cold temperature extremes, transient dynamic loads like hull-slamming and complex three-dimensional hydrodynamic loads. These structures are also required to withstand weapon impact and blast loads resulting from surface and underwater explosions. Recent assessments of marine structures have demonstrated that sandwich composites can provide good blast mitigation due to their high strength-to-weight ratios and high shear-and-bending resistances. Characterization of the behavior of these composite materials and polymeric foams under impulsive loading is a prerequisite for the analysis and design of effective, blast-resistant structures.

Damage and deformation due to dynamic loading in layered materials such as composite laminates has been the subject of numerous investigations in recent years. Initial studies focusing on damage under quasi-static and low-velocity impact loading have

[1]To whom correspondence should be addressed, Tel: 404-894-3294, Fax: 404-894-0186, Email: min.zhou@gatech.edu, also with WCU Program on Multiscale Mechanical Design, School of Mechanical and Aerospace Engineering, Seoul National University, Seoul, Korea

revealed the basic processes of damage initiation and evolution. The mechanisms of damage under low-velocity impact include matrix-cracking, fiber-breakage and interlaminar delamination, primarily due to transverse shear-stresses [1–3]. Of these mechanisms, delamination is by far the most detrimental to stiffness and strength and is a major concern. The damage behavior of composite laminates is significantly influenced by matrix-material, stacking sequences and thickness. Property mismatch in layered materials is one cause for delamination [4–6]. Chang and coworkers have studied the damage behavior of composite laminates under gas-gun based impact loading, concluding that in-ply matrix cracking occurs first followed by delamination growth and shear-and-bending crack initiation [7–9]. Minnaar and Zhou [10] developed novel laser-interferometric diagnostics and showed that interlaminar crack speeds were significantly higher under shear loading, and that crack speeds were strongly influenced by loading rate in mode-II cracks. However, only limited work has been reported in the literature [11, 12] on the dynamic response of composites to water-based impulsive loads.

By combining a thick and soft core and thin facesheets, sandwich structures achieve considerably high shear-stiffness-to-weight ratios and bending-stiffness-to-weight ratios than equivalent homogeneous plates made exclusively of either the core material or the facesheet material. The primary factors that influence the structural response of a sandwich structure are (1) facesheet thickness, (2) core thickness and (3) core density. Zenkert [13] provided a review of the mechanics of sandwich structures, expanding on the previous work of Plantema [14] and Allen [15]. The bulk of previous research on the dynamic behavior of sandwich composites has focused on low-velocity contact-based loads such as drop weight and projectile impact [16–22]. Tekalur and Shukla [23] examined the dynamic response of woven E-glass composite facesheets and stitched core sandwich structures to air-based shock loading and concluded that stitched cores exhibit superior mechanical performance. Espinosa et al. simulated the effects of underwater blasts by impacting a projectile on a piston in contact with water [24, 25] and concluded that steels may be preferred when maintenance of residual strength is a priority and composite materials make better low-weight blast-resistant hulls. The use of explosives to generate underwater impulsive loads has also been reported [26–28].

So far, the relationship between performance in terms of failure-resistance and energy dissipation and design parameters of heterogeneous sandwich structures have not been well quantified, primarily due to the lack of experimental diagnostics and quantitative structural simulations under various conditions. Because of the inherent heterogeneity of sandwich composites, there exist several competing failure mechanisms such as delamination and matrix cracking in the laminates, core-face debonding, core compression and core cracking. The material properties of the different components significantly affect the blast resistance of the structures. In addition, loading conditions (load intensity, boundary conditions, and loading environments) influence the failure modes. Clearly, the failure mechanisms in sandwich composites are complex and a systematic study is needed to develop performance-design relations.

This study focuses on the blast resistance and energy absorption of sandwich composites with varying core densities subjected to underwater impulsive loading. Three different PVC foams are used in sandwich: Divinycell HP60, HP100 and HP200. The composite laminates used for the facesheets are E-glass/Polyester with a bi-axial layup. For comparison, a monolithic composite plate made of the same E-glass/polyester composite laminate is also analyzed. In order to facilitate comparison of dynamic response, all structures are designed to have the same total areal mass of ~10.5 kg/m$^2$. Simulations are carried out for a range of impulsive load intensity and two distinct loading

configurations: (1) air-backed configuration with the structure in contact with water on the impulse side and (2) water-backed configuration with the structure in contact with water on the impulse side as well as the backside. The focus is on characterizing the blast resistance of sandwich composites as a function of loading intensity and structural attributes. The objective is to identify deformation mechanisms leading to ultimate failure and develop material-property-performance relations to aid the development of blast resistant marine structures. Although this research involves experiments as well as simulations, this paper is primarily concerned with the numerical results. Details about the experiments are provided elsewhere [29, 30].

## 2. EXPERIMENTAL CONFIGURATION

Gas gun impact has been successfully used to generate impulsive loading through water [29–31]. To obtain controlled loading and simulate various water-structure contact scenarios, we have designed and fabricated an experimental facility called the Underwater Shock Loading Simulator (USLS) which allows a variety of load configurations to be studied with quantitative diagnostics. Important features of this facility include the ability to generate water-based impulsive loading of a wide-range of intensities, the ability to simulate the loading of submerged structures, and integrated high-speed photographic and laser interferometric diagnostics. This facility is used in conjunction with computational modeling. Figure 1(a) and (b) shows schematic illustrations of the air-backed and water-backed loading configurations analyzed. The shock tube is an 800 mm long cylinder which is horizontally mounted and filled with water. It is made of steel and has an inside diameter of 80 mm. A thin piston plate is mounted at the front (left) end and the specimen is located

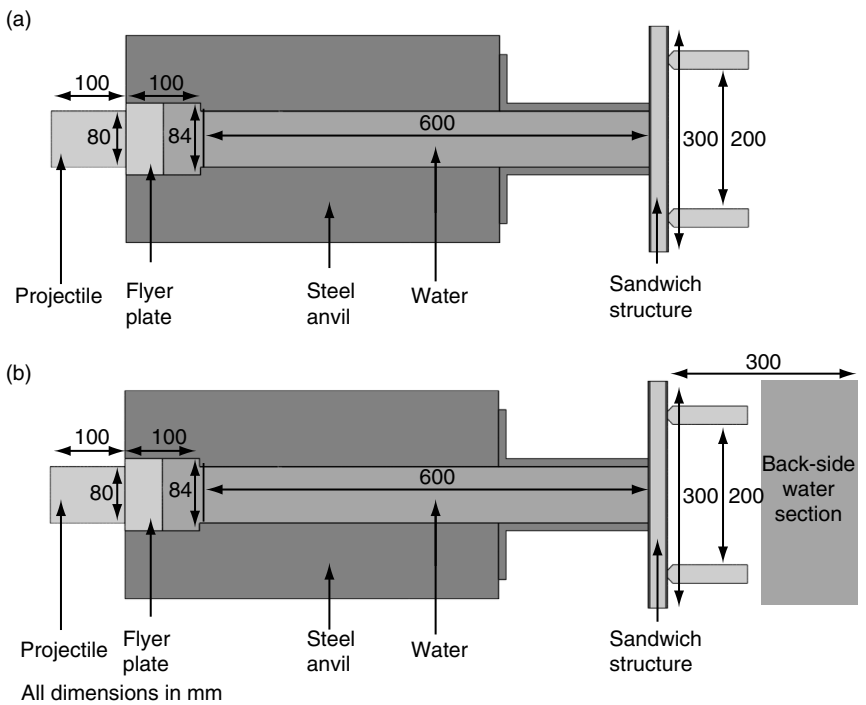


Figure 1 Schematic illustration of the of USLS and simply-supported sandwich structure in (a) air-backed and (b) water-backed configurations.

at the rear (right) end. A projectile is accelerated by the gas gun and strikes the piston plate, generating a planar pressure pulse in the shock tube. This pulse travels down the shock tube and impinges upon the specimen. The target is supported by an anvil which is bolted to an I-beam.

According to Taylor's analysis of one-dimensional blast waves [32], for a plane wave impinging on a free-standing plate, the pressure in the fluid at a fixed position follows the relation

$$p(t) = p_0 \exp\left(-\frac{t}{t_0}\right), \tag{1}$$

where $P_0$ is the peak pressure, $t$ is time and $t_0$ is the decay time. The area under this curve is the impulse imparted by the wave

$$I = \int_0^t p\left(t\right) dt. \tag{2}$$

A non-dimensionalized impulse $\bar{I}$ can be expressed as

$$\bar{I} = \frac{I}{\rho_w c_w \sqrt{A}}, \tag{3}$$

where $\rho_w$ is the density of water, $c_w$ is the speed of sound water in water and $A$ is the area of loading. Impulsive waves due to underwater blasts have a characteristic decay time on the order of $\sim 10^{-4}$ seconds. The experimental facility and numerical modeling simulate the effects of different stand-off distances of an explosive source. Tri-Nitro Toluene (TNT) is used to calibrate underwater blasts. For an underwater explosion, the peak pressure (in MPa) scales as

$$p_0 = 52.4\left(\frac{M^{1/3}}{r}\right)^{1.13}, \tag{4}$$

where $p_0$ is the mass of TNT in kilograms and $r$ is the standoff distance in meters [32–34].

In the experiments, pressures ranging from 10 MPa to 300 MPa can be generated using different projectile velocities. Pressures are measured using dynamic pressure transducers capable of measuring peak pressures up to 500 MPa. The rise time of the pressure pulses is on the order of 25 μs and the decay time is on the order of 800 μs. The impulsive loads considered in this set of calculations have the peak pressures of 175, 140, 90 and 40 MPa which approximately correspond to 1 kg of TNT exploding at distances of 350, 425, 620 and 1250 mm respectively. The impulse magnitudes calculated using eqn. (3) are $\bar{I}$ = 0.015, 0.035, 0.055, and 0.065. Figure 2(a–d) shows a comparison of experimentally and numerically measured pressure histories corresponding to four different projectile velocities. The solid lines show experimentally measured pressure histories while the dotted lines show the numerically calculated pressure histories. The peak pressures and decay times measured in experiments and calculated in numerical simulations are in good agreement.

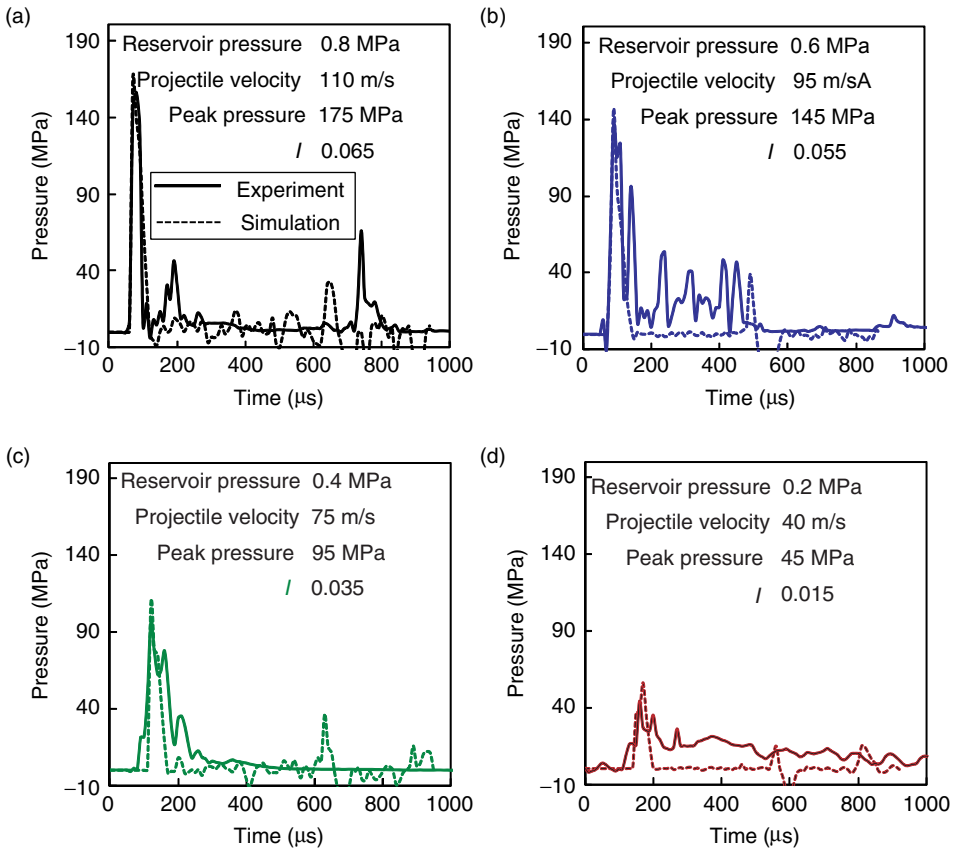


Figure 2 Comparison of numerical and experimental pressure histories in the water-chamber for four different projectile velocities and impulse magnitudes $\bar{I}$ = 0.015, 0.035, 0.055 and 0.065.

## 3. STRUCTURES ANALYZED

A simply-supported loading configuration is used because the location of the failure modes in this configuration allows accurate time-resolved measurements using high-speed digital imaging. Specifically, a high-speed digital camera can be used to study the overall deflection, face-wrinkling, core-face debonding, core-compression, core shear-cracking and rupture. The facesheets are made of bi-axial $[090]_s$ E-glass/Polyester composites and the core is PVC foam manufactured by DIAB Inc[35]. Three PVC foam densities are used: HP60, HP100, HP200. Sandwich structures analyzed here are in the form of beam specimens of length 300 mm and width 80 mm. The facesheet thickness is 3 mm and the core-thicknesses are modified to keep the total mass of all structures the same. The core thickness of the HP60, HP100 and HP200 are 10, 20 and 30 mm respectively. The facesheets and cores are joined using an epoxy adhesive. Figure 3 illustrates the composite structures analyzed. This sample size is approximately one order of magnitude smaller than composite sections used in ships, giving reasonable representation of marine composite structures. To compare the effect of varying core density on dynamic response, a relative density in the form of

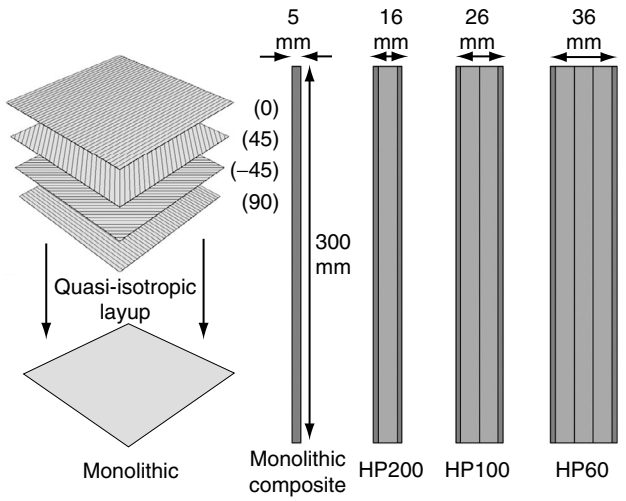


Figure 3 Schematic illustration of a sandwich structure with length $L$, core-thickness $T_C$, and front and back face thickness $T_F$. The total areal mass of all structures analyzed is the same.

$$\bar{\rho} = \frac{\rho_{core}}{\rho_{PVC}} \tag{5}$$

is used. For the monolithic composite (which does not have a PVC foam core), the relative density is

$$\bar{\rho} = \frac{f_{matrix} \cdot \rho_{matrix}}{f_{fiber} \cdot \rho_{fiber}}, \tag{6}$$

where $f_{matrix}$ and $\rho_{matrix}$ are the volume fraction and density of the matrix respectively and $f_{fiber}$ and $\rho_{fiber}$ are the volume fraction and density of the reinforcement respectively.

In a large naval structure, like a ship or a submarine, there are a number of different loading conditions and environments. For example, ship hulls and superstructures consist of water on the outer side (impulse side) and air or machinery on the inner side. Conversely, the keel, rudder, propeller blades and underwater pipelines consist of water on both the impulse side and the protected side of the structure. For the purpose of the current study, the former is called the air-backed configuration [Figure 1(a)] and the latter is called the water-backed configuration [Figure 1(b)].

The composite structures are subjected to impulsive loading at its center as shown in Figure 1(a and b). The impulsive waves are planar and produce a uniform load across the width of the specimen, simplifying the damage processes to a 2-D event. The loading configuration is designed to account for a range of loading rates and load triaxiality. The simply supported configuration closely resembles the conditions created by hull stiffeners. The impulsive loads that impinge on the target create strain rates up to $10^4$ $s^{-1}$.

## 4. NUMERICAL FRAMEWORK

The numerical model explicitly accounts for the projectile, piston plate and water column in contact with the sandwich plate target. The projectile is prescribed with an initial velocity $V_0$. Simulations are carried out with a Lagrangian description for the water and target. Since the Lagrangian framework produces water-structure interactions and accurate pressures and impulses, we use this framework for the current set of calculations.

The finite element framework uses linear 4-noded bulk elements. A $[0, 90]_S$ layup is specified for each ply in the facesheets. For the composite material and PVC foams, an element is deleted if internal damage exceeds a pre-determined threshold. A master-slave contact algorithm is used for interactions between the facesheets and core and a non-penetrating, general contact algorithm is implemented at projectile-piston, piston-water and water-sandwich structure interfaces. Cohesive elements are used at the core-facesheet interface to simulate core-facesheet debonding [36, 37]. A bilinear cohesive law is implemented, accounting for mixed-mode failure at interfaces. Post-failure, the normal penalty-contact algorithm is enforced to prevent interpenetration.

### 4.1. CONSTITUTIVE AND DAMAGE MODELS FOR PVC FOAMS

The core is made of Divinycell H-100 PVC foam [35]. The response consists of three distinct regimes: (1) initial nearly elastic deformation; (2) plateau region in which deformation occurs at relatively constant stress; and (3) lock-up/densification stage beyond which the material becomes fully compacted, as shown in Figure 4. The constitutive model adopted for Dinvinycell PVC foam is the one developed by Deshpande and Fleck [38, 39] and implemented in the current finite element code Abaqus [37]. The model accounts for isotropic, dilatational plasticity. High strain-rate studies on PVC foams show a weak dependence on strain-rate [40]. Hence, the foam is assumed to be strain-rate independent in

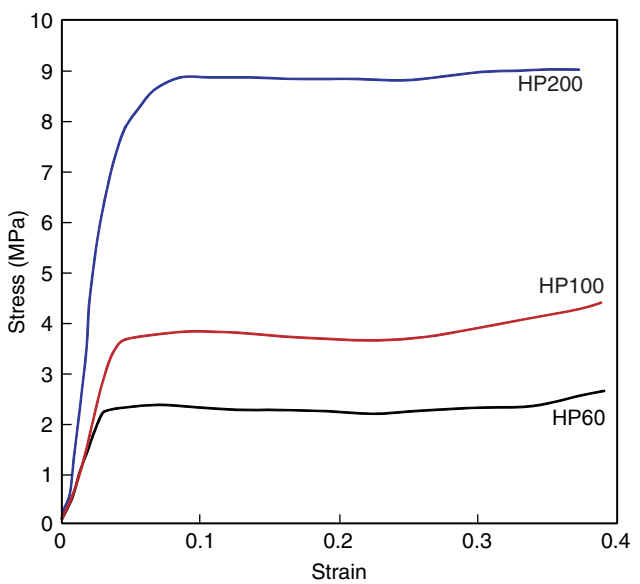


Figure 4 Stress-strain curves of HP60, HP100 and HP200 at a strain-rate of ~1000 $s^{-1}$.

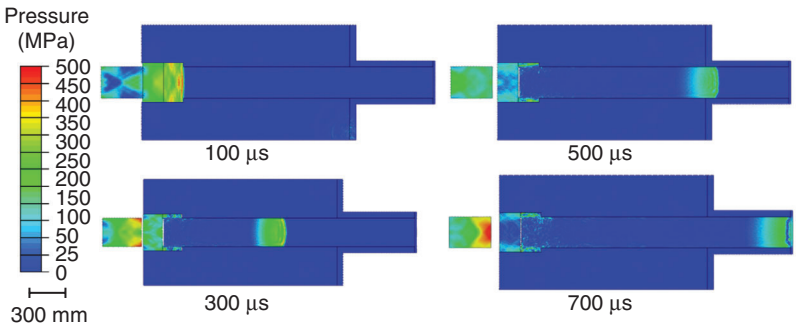


Figure 5 Distributions of pressure for an impulsive wave generated in the water-chamber when a projectile velocity travelling at 75 m/s strikes the flyer plate.

the current set of numerical simulations. The equivalent yield stress $\hat{\sigma}$, based on uniaxial testing, is given by

$$\hat{\sigma}^2 = \frac{1}{1+\left(\alpha/3\right)^2}\left(\sigma_e^2 + \alpha^2\sigma_m^2\right), \tag{7}$$

where $\hat{\sigma}$ is a function of effective stress $\sigma_e$ and hydrostatic stress $\sigma_m$, such that

$$\sigma_e = \sqrt{\frac{3}{2}\tau_{ij}^{'}\tau_{ij}^{'}}, \sigma_m = \frac{1}{3}\sigma_{ii}, \text{ and } \alpha = \sqrt{\frac{9}{2}\left(\frac{1-2\nu}{1+\nu}\right)}, \tag{8}$$

and $\alpha$ is the parameter that determines the shape of the yield surface and $\nu$ is Poisson's ratio. Material parameters for the PVC foams are listed in Table 1.

While previous constitutive models used for polymeric foams have not included damage or fracture criteria, experimental results show that shear-fracture and fragmentation are significant deformation mechanisms and cannot be neglected in numerical simulations. Here, a phenomenological damage criterion proposed by Hooputra et al. [41] is implemented to predict the onset of fracture due to shear-localization and to capture the subsequent fragmentation. The damage criterion assumes that equivalent plastic strain $\bar{\varepsilon}_D^{pl}$ at the onset

Table 1 Constitutive parameters for core materials [35].

| Parameter | Unit | HP60 | HP100 | HP200 |
|---|---|---|---|---|
| Density | kg/m$^3$ | 65 | 100 | 200 |
| Tensile modulus | MPa | 20 | 100 | 250 |
| Tensile strength | MPa | 1.8 | 3.5 | 7.1 |
| Compressive modulus | MPa | 74 | 135 | 310 |
| Compressive strength | MPa | 0.95 | 2.0 | 5.4 |
| Shear modulus | MPa | 20 | 33 | 73 |
| Shear strength | MPa | 0.85 | 1.6 | 3.5 |

of damage is dependent on stress-triaxiality and strain-rate $\left[\bar{\varepsilon}_D^{pl}\left(\eta, \dot{\bar{\varepsilon}}^{pl}\right)\right]$ where $\eta = -p/q$ is the stress triaxiality, $p$ is the pressure stress, $q$ is the Mises equivalent stress and $\dot{\bar{\varepsilon}}^{pl}$ is the equivalent plastic strain-rate. The fracture-properties of the parent material (in this case PVC) are used in the damage criterion. The criterion for damage initiation is

$$\omega_D = \int \frac{d\bar{\varepsilon}^{pl}}{\bar{\varepsilon}_D^{pl}\left(\eta, \dot{\bar{\varepsilon}}^{pl}\right)} = 1, \tag{9}$$

where $\omega_D$ is a state variable which increases monotonically with plastic deformation.

While the ductile-damage criterion is phenomenological, it is a useful addition to the finite element model because it enables the tracking of core-cracking and fragmentation. The inclusion of a damage criterion has significant implications for energy dissipation and dynamic response.

## 4.2. CONSTITUTIVE AND DAMAGE MODELS FOR COMPOSITE LAMINATES

Composite laminate faces are considered to be perfectly elastic until the onset of damage. Damage occurring in the facesheets is accounted for by an energy-based damage evolution law proposed by Hashin [11, 42]. In finite element simulations, a material-point has an initial, undamaged value of 1 and as the material-point experiences damage, this value decreases. The lowest value is 0, after which the element is removed from the simulation. The parameters used in these calculations can be found in [22, 43] and are shown in Table 2.

## 4.3. EQUATION OF STATE FOR WATER

A Lagrangian formulation is adopted to simulate wave propagation in water. It captures the exponentially decaying pressure waves and cavitation at the fluid structure interface. The response of water is described by the Mie-Gruneisen equation of state such that

$$p = \frac{\rho_0 c_0^{\,2} \eta}{(1 - s\ \eta)^2}\left(1 - \frac{\Gamma_0 \eta}{2}\right) + \Gamma_0 \rho_0 E_m, \tag{10}$$

Table 2 Material parameters for facesheets (E-Glass/Polyester).

| **Parameter** | **Unit** | **Value** |
|---|---|---|
| Density | kg/m$^3$ | 2100 |
| Tensile modulus | MPa | 44000 |
| Transverse modulus ($E_Y$) | MPa | 9000 |
| Shear modulus ($G_{XY}$, $G_{XX}$, $G_{YX}$) | MPa | 4000 |
| Longitudinal tensile strength | MPa | 2500 |
| Longitudinal compressive strength | MPa | 2000 |
| Transverse tensile strength | MPa | 75 |
| Transverse compressive strength | MPa | 150 |
| Longitudinal shear strength | MPa | 75 |
| Transverse shear strength | MPa | 75 |

Table 3 Parameters for the Mie-Gruneisen equation of state for water.

| Parameter | Unit | Value |
|---|---|---|
| Density of water | $kg/m^3$ | 1000 |
| Speed of sound in water | m/s | 1500 |
| Gruneisen's Gamma | — | 0.1 |
| $s = dU_s/dU_p$ | — | 1.75 |

where $p$ is the current pressure, $c_0$ is the speed of sound, $\rho_0$ is the initial density, $E_m$ is internal energy per unit mass, $\Gamma_0$ is Grüneisen's Gamma at a reference state, $s = dU_s/dU_p$ is the Hugoniot slope coefficient, $U_s$ is the shock wave velocity and $U_p$ is the particle velocity which is related to $U_s$ through a linear Hugoniot relation

$$U_S = c_0 + sU_p . \tag{11}$$

The values of the constants used in eqns. (10) and (11) are listed in Table 3.

## 5. RESULTS AND DISCUSSIONS

A parametric study is carried out, focusing on the effects of (i) loading intensity, (ii) changes in core properties (monolithic, HP60, HP100, and HP200), and (iii) air-backed and water-backed configurations. For all the calculations presented, simply-supported boundary conditions are used. Four different projectile velocities are used to generate impulsive loads that are imposed on the central area of the specimen. Since the load is distributed rather uniformly across the width of the specimen, damage and deformation can be accurately tracked using a 2-D numerical framework. The deflection and energy dissipation in the monolithic plate are taken as benchmarks and the deflection and energy dissipation in the sandwich structures are compared to the benchmarks.

### 5.1. DYNAMIC DEFORMATION AND FAILURE MECHANISMS

Figure 6 shows a comparison of high-speed photographs from experiments and contour plots for damage from simulations at different times for a structure with HP60 core subjected to $\bar{I}$ = 0.035. Experiments reveal that core-compression commences immediately after the onset of loading at $t$ = 150 μs and inclined cracks originate near the loading circumference. These cracks propagate from the front-face to the back-face and branch into three branches (at $t$ = 450 μs ) near the back-face and lead to core-back face debonding. Core indentation is observed at the center. Core compression and core cracking occur simultaneously with crack propagation through the core. Core face debonding is observed at $t$ = 600 μs.

The contour plots of damage at four successive time steps after the onset of loading are shown in Figure 6. At $t$ = 150 μs, the impulsive load is transmitted through the facesheet and core cracking initiates. The flexural waves in facesheets travel faster than the flexural waves in the core which causes core-front face debonding. Initially, core compression is elastic and completely recoverable. At $t$ = 300 μs. core crushing (permanent, inelastic deformation) is observed in the central region and cracks propagate towards the supports. These cracks tend to follow the directions of principal shear stresses in the specimen. Crack branching and fragmentation occur at $t$ = 450 μs. While damage in the front-face is widespread, the back-face is relatively undamaged. The entire structure achieves a common velocity at $t$ = 600 μs.

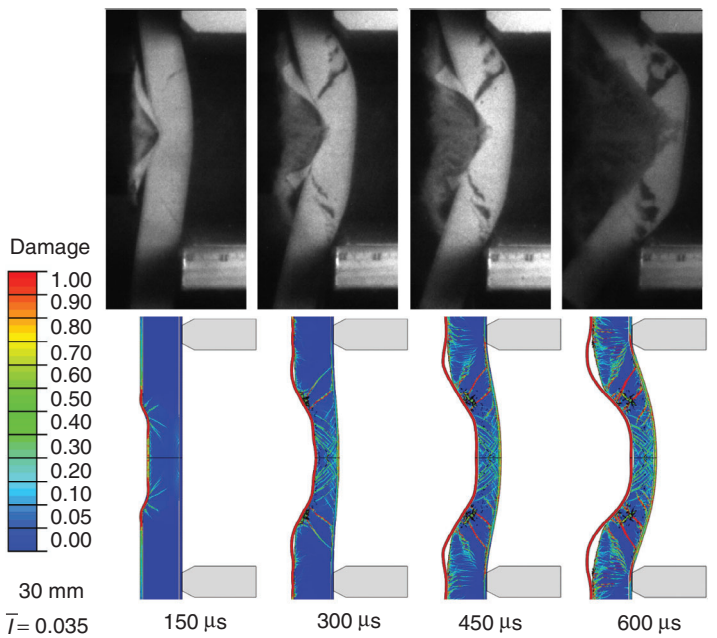


Figure 6 Comparison of experimental and calculated deformation sequences for a sandwich structure with HP60 core subjected to $\bar{I}$ = 0.035. The major deformation mechanisms, i.e., core-cracking, core-front face debonding and core-crushing, are captured in the finite-element simulations.

The numerical simulations accurately depict the different failure modes observed in experiments. Maximum damage occurs close to the loading area and spreads outward in later stages of the loading event. The major deformation modes in the sandwich structure can be divided into distinct regimes based on the time required for each regime: (1) load transfer through front face and onset of core compression; (2) elastic and inelastic core compression; (3) core cracking and fragmentation and load transfer to back face; and (4) bending in entire structure. The material properties of the sandwich core determine the duration of each regime.

To illustrate the deformation and damage in different composite structures, the distributions of damage due to matrix cracking and core cracking and fragmentation are shown in Figure 7 for $\bar{I}$ = 0.035 at $t$ = 600 µs In the monolithic composite, matrix cracking is observed near the circumference of the loading area. Significant damage occurs in the composite layers that are in contact with water. The back face of the monolithic composite is relatively undamaged. In the sandwich composite with the HP200 core, core front face and back face debonding occurs over the entire structure and the core fails through shear cracking. Both the front face and the back face experience significant damage. In the sandwich composite with the HP100 core, the front face experiences significant damage and core front face debonding is observed. In the sandwich composite with the HP60 core, front face buckling and core-front face debonding are observed; but the back face is relatively undamaged. It is apparent that damage in the back face is highly dependent on the properties of the core. Clearly, damage and failure in simply supported sandwich structures occur primarily through the formation of discrete 45° core cracks and separation along the core

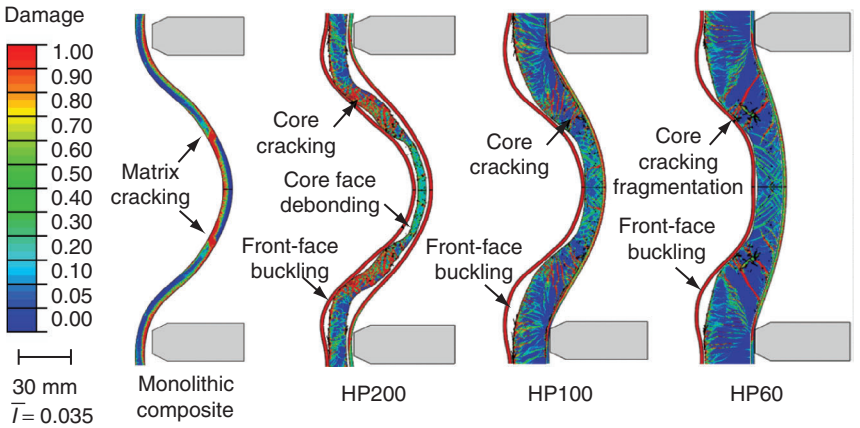


Figure 7 Distributions of damage in air-backed monolithic composite and sandwich structures with HP60, HP100 and HP200 cores. Projectile velocity is 75 m/s and $\bar{I}$ = 0.035.

face interface. Structural failure in all cases is due to from shear stresses near the loading area and bending stresses near the supports.

## 5.2. DEFLECTION

In response to the impulsive wave incident on the front face, a stress wave propagates through the front face, core and back face in the direction parallel to the impulsive load. Since the specimen is simply supported near the edges, bending deformation initiates after the onset of loading. The midpoint of the back face in all structures experiences the highest deflection. This deflection ($\Delta/L$) is taken as a measure of structural deformation.

Figure 8 shows the histories of center displacements normalized by the length of the structure (300 mm) for front and back faces of the sandwich panels along with those of the equivalent weight monolithic composite as a function of time for structures with (a) HP60, (b) HP100, and (c) HP200 cores. The center displacement of the monolithic composite is higher than those of all sandwich structures. The velocity acquired by the monolithic plate is essentially the same as that of the front face in all three cases. For all three core densities, the front face acquires much higher velocities than the back face. The deformation in the back face is a result of core crushing and load transfer through the core. For the HP200 core, the displacement in the back face occurs after a delay of 50 μs. Comparison of the deflections for front and back faces shows that both faces move with the same velocity. The back face deflection for this case is ~6% lower than the deflection in the monolithic composite. For the HP100 core, the displacement in the back face occurs after a delay of 75 μs and the back face experiences ~30% lower overall displacement compared to the monolithic composite. For the HP60 core, displacement in the back face occurs after a delay of 100 μs and the back face deflection is ~60% lower than the deflection in monolithic composite. The shaded regions in the plots show the core compression for each case. As the core relative density increases, core compression decreases significantly. Comparison of back face and monolithic composite plate displacements indicate that sandwich structures provide significant benefits for blast resistance.

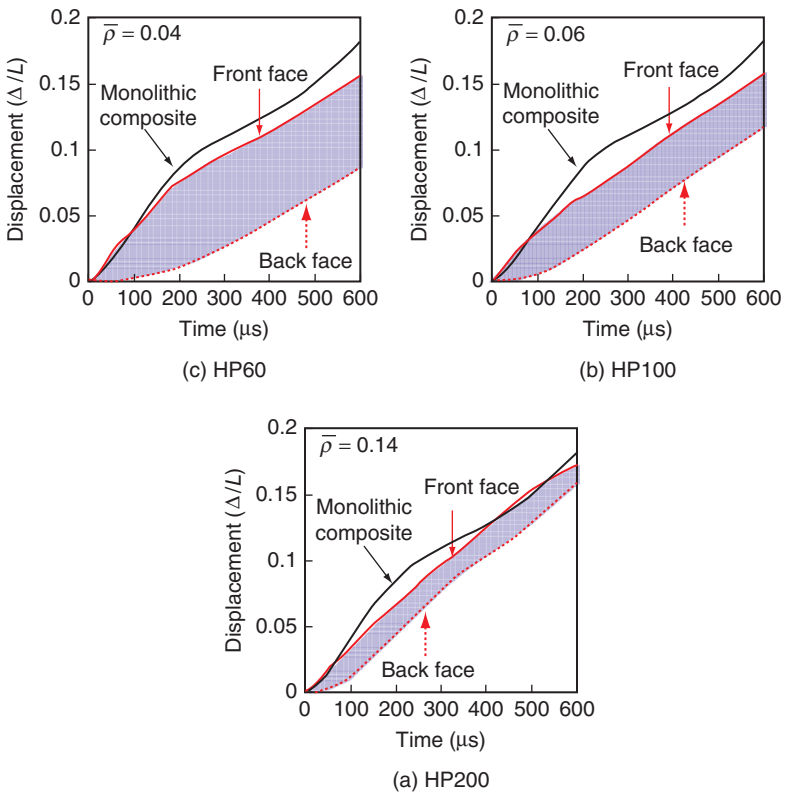


Figure 8 Front and back face displacements as functions of time for air-backed sandwich structures with (a) HP200, (b) HP100, and (c) HP60 cores subjected to $\bar{I}$ = 0.035. The shaded region is the core compression in each case. The solid black line denotes the displacement of the monolithic composite.

Figure 9 shows the normalized deflections ($\Delta/L$) for all 16 configurations as functions of impulse $\bar{I}$ and relative density $\bar{\rho}$. The vertical axis shows the normalized deflection. At all impulse magnitudes, structures with the lowest relative density experience the least deflections. The deflections increase with increasing relative density as well as impulse magnitudes. HP200 cores perform only marginally better than monolithic structures. HP100 and HP60 cores exhibit significantly higher blast resistances in comparison to HP200 core and the monolithic composite. The relationship between deflection in air-backed structures ($\Delta/L_{AB}$), and incident impulse ($\bar{I}$)and relative density ($\bar{\rho}$) can be given by

$$\Delta/L_{AB} = 16.54 \cdot \bar{\rho}^{(0.45)} \cdot \bar{I}^{(1.28)}. \tag{12}$$

It should be noted that as the relative density increases, the thickness of the sandwich structure decreases, as shown in Figure 3.

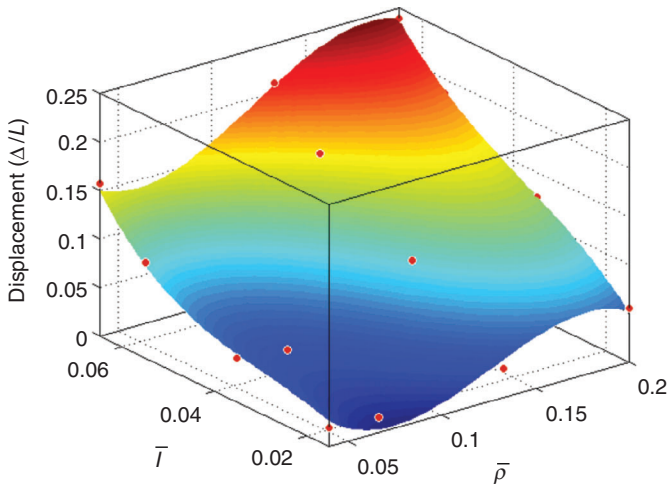


Figure 9 Normalized displacement in air-backed structures as function of incident impulse $\bar{I}$ and core relative density $\bar{\rho}$.

## 5.3. ENERGY DISSIPATION

There are two modes of energy dissipation in the structures, i.e., inelastic deformation and damage in composite laminates, irrecoverable core compression, core cracking and fragmentation. The total energy dissipation is the sum of the contributions from these modes of dissipation. The exact proportion of the energy dissipated by each mode depends on the relative density of the core and the dimensions of the structural components.

Figure 10(a–d) shows energy dissipation as a function of time in the front face, core and back face for the four different structures subjected to $\bar{I}$ = 0.035. It can be seen that monolithic composites show the highest energy dissipation, which can be attributed to their extensive deformation and damage. On the other hand, the energy dissipated due to damage in the front face is rather similar for all the sandwich structures and is ~20% of the total energy dissipated. As discussed previously, HP200 cores undergo severe damage and deformation resulting in high energy dissipation in the core. When the front face fails and core compresses, the back face experiences impulsive loads and undergoes damage and contributes to the overall energy dissipation. For HP100 and HP60, core damage is less severe and the back face is relatively undamaged. Comparing the slopes of energy dissipation versus time relation in the first 100 μs shows that the rate of energy dissipation is the highest in HP200, followed by HP100 and HP60.

Figure 11 shows the evolution of the kinetic energy and energy dissipation in the different sandwich cores due to inelastic deformation and damage for $\bar{I}$ = 0.035. The dotted line shows the kinetic energy imparted to the sandwich structures, which is rather similar in all cases. The maximum energy absorbed by the HP200 core is ~1.51 J of which the damage dissipation energy is ~2% and inelastic dissipation energy is ~98%. For both HP100 and HP60 cores, damage dissipation is negligible and inelastic dissipation is the dominant energy absorption mechanism. Of the incident kinetic energy, the HP200, HP100 and HP60 cores absorb 75, 60 and 50%, respectively. As the core relative density increases, the kinetic energy acquired by the core increases monotonically. Additionally, the rate of energy dissipation is higher for sandwich cores

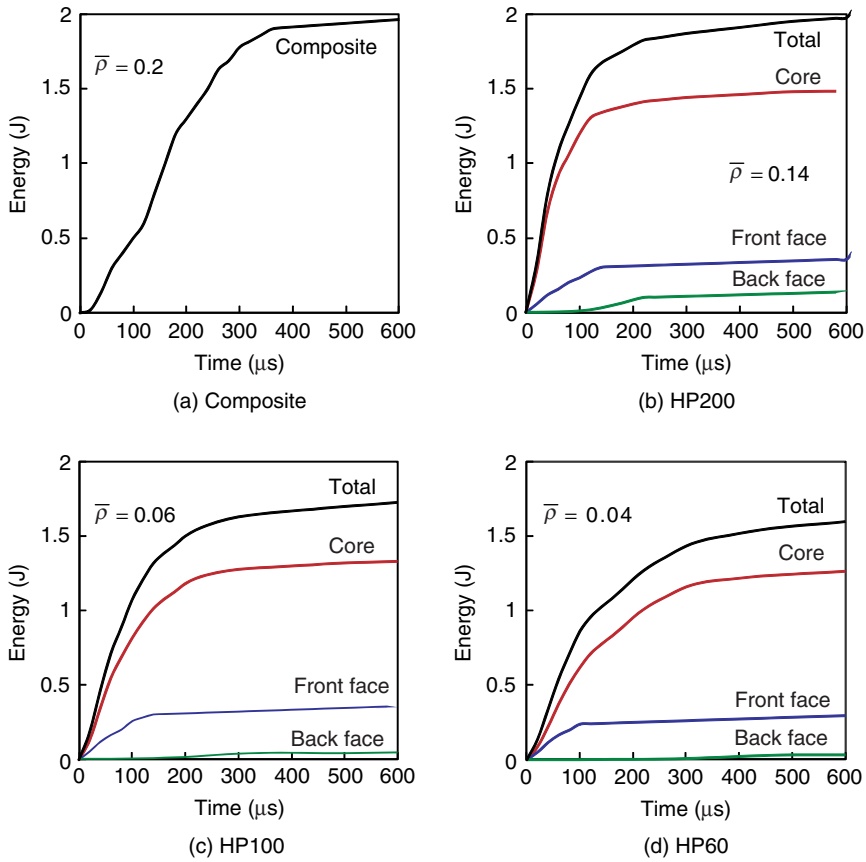


Figure 10 Energy dissipation due to inelastic deformation in different components of the sandwich structures for $\overline{I}$ = 0.035.

with high relative densities. Due to the higher energy dissipation rate, cores with high relative densities undergo more severe cracking and fragmentation. Clearly, sandwich cores which reduce the magnitude and rate of load transfer provide higher blast mitigation.

The energy dissipation for all 16 configurations as a function of impulse ($\overline{I}$) and relative density ($\overline{\rho}$) is shown in Figure 12. The energy dissipation in sandwich structures is strongly influenced by both core relative density and impulse magnitude. Monolithic composite laminates consistently dissipate higher amounts of energy in comparison to the sandwich structures. The variation of energy dissipation in air-backed structures ($E_{AB}$) can be quantified using the non-dimensional terms $\overline{I}$ and $\overline{\rho}$ as,

$$E_{AB} = 657 \cdot \overline{\rho}^{(0.38)} \cdot \overline{I}^{(1.01)} . \tag{13}$$

While structures with low relative densities exhibit low deflections, these structures also exhibit lower energy absorbency compared to those with high relative densities. The fact that

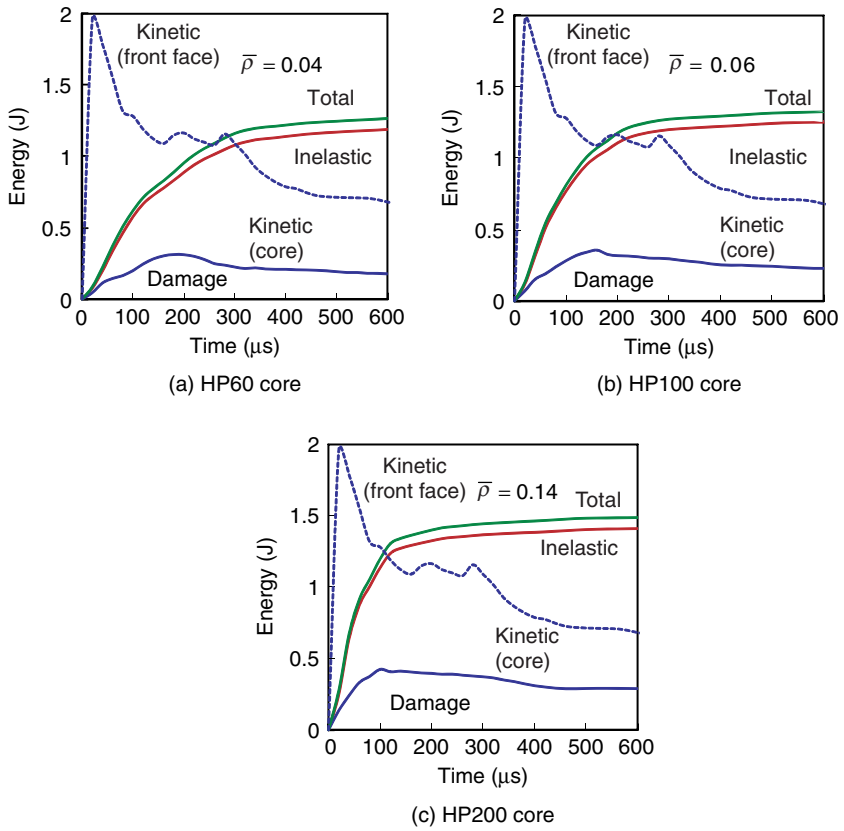


Figure 11 Energy dissipation in core materials as a function of time for $\overline{I}$ = 0.035.

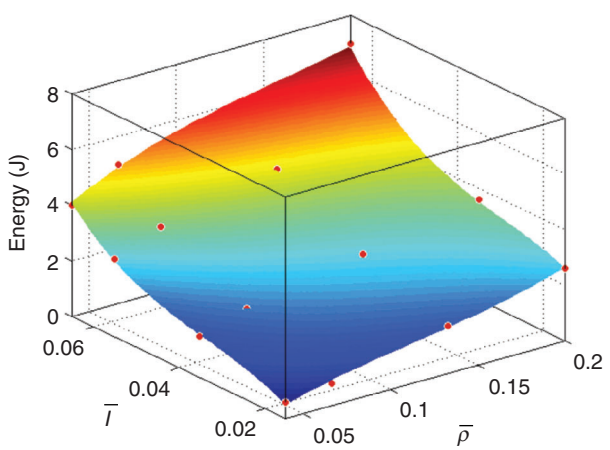


Figure 12 Energy dissipated due to inelastic deformation in air-backed structures as a function of incident impulse $\overline{I}$ and core relative density $\overline{\rho}$.

structures which dissipate more energies also exhibit higher deflections indicates that the internal failure modes in the sandwich structures have a considerable effect on dynamic response. Alleviating the effects of damage mechanisms in the sandwich structure can significantly improve overall blast resistance.

## 5.4. RESPONSE OF WATER-BACKED STRUCTURES

The previous section focused on the deformation and failure modes, load-carrying capacity and energy dissipation of air-backed structures. In addition to the results reported so far, a set of simulations is carried out to investigate the role of water contact on both sides of the structure. Figure 13 shows the distributions of damage in four different composite structures in water-backed loading configuration [Figure 1(b)] for $\bar{I}$ = 0.035. These contour plots illustrate the differences in the behavior of air-backed and water-backed structures. For the monolithic composite, high shear stresses develop near the circumference of the loaded area, causing severe damage in the form of matrix cracking. For the sandwich structures however, flexural waves in the front face cause core-front face debonding and front face buckling. Damage is localized and the structure is relatively undamaged in regions that are away from the loading area. Clearly, for all structures, the overall deflection under water-backed conditions is severely restricted due to the presence of the back-side water. Due to the lack of overall deflection and bending, tensile loads in both faces are negligible and the faces undergo significantly lower damage in comparison to the corresponding air-backed cases.

To evaluate the role of relative density on dynamic response, the time histories of center displacements experienced by the monolithic composite and both faces in the sandwich structures are shown in Figure 14. The shaded region illustrates the core compression in each case. Core compressive strains for all cores are similar (~100%), but the absolute core compression is significantly higher for HP60 than for HP100 and HP200. For the sandwich structures, due to low core relative densities, the front face starts moving with a higher velocity than the monolithic plate and the front face velocity

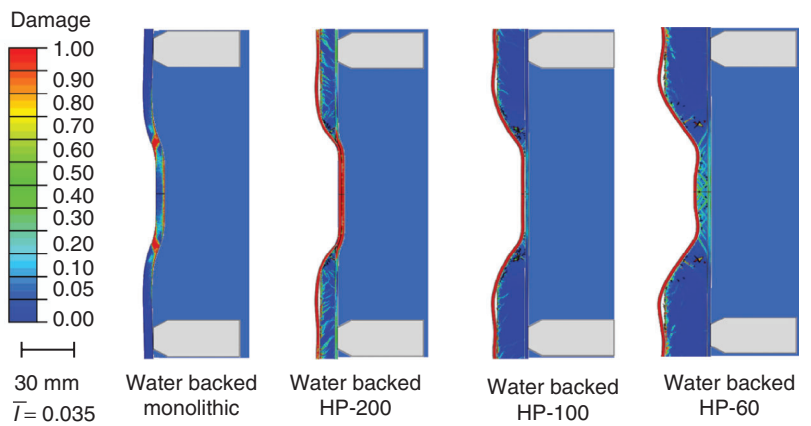


Figure 13 Distributions of damage in water-backed monolithic composite and sandwich structures with HP60, HP100 and HP200 cores. Projectile velocity is 75 m/s and $\bar{I}$ = 0.035.

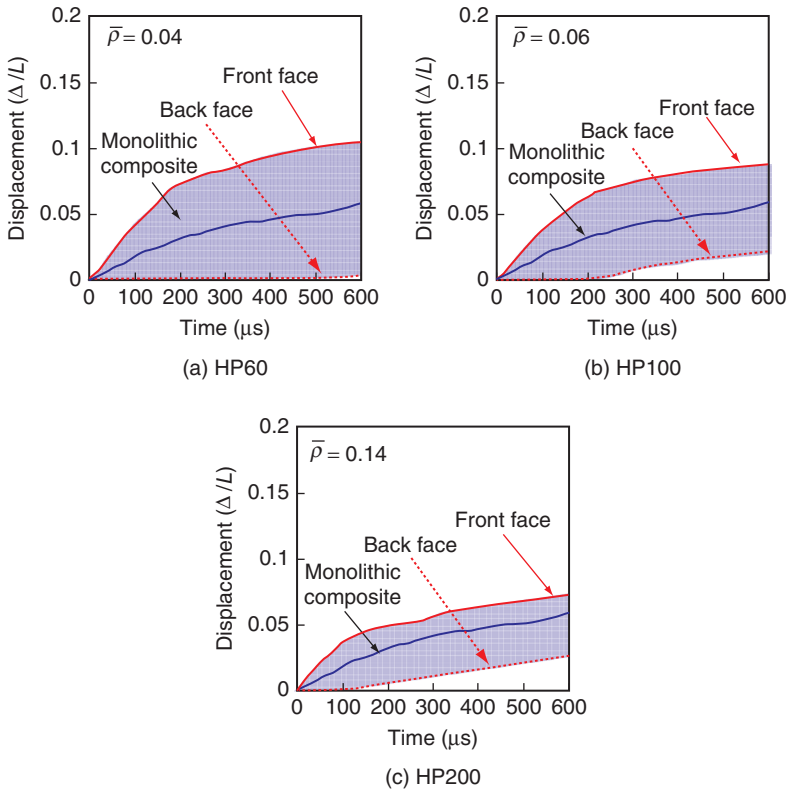


Figure 14 Front and back face displacements as functions of time for water-backed sandwich structures with (a) HP60, (b) HP100, and (c) HP200 cores subjected to $\bar{I}$ = 0.035. The shaded region is the core compression in each case. The solid black line denotes the displacement of the monolithic composite.

is limited by the core. Therefore, the momentum transferred to the core increases with increasing core relative density. Comparison of the overall displacements in the sandwich structures to that in the monolithic composite shows that the HP200, HP100 and HP60 cores experience 60, 70 and 90% lower displacements respectively. As observed in air-backed structures, thick cores with low relative density provide the highest blast mitigation. In the water-backed case, on average, the deflections are 50% lower than the deflections in the air-backed case.

Figure 15 shows the normalized deflections ($\Delta/L$) for all 16 unique configurations for the water-backed case as functions of impulse ($\bar{I}$) and relative density ($\bar{\rho}$). The relationship between overall deflection ($\Delta/L_{WB}$) and $\bar{I}$ and $\bar{\rho}$ is given by

$$\Delta/L_{WB} = 19.43 \cdot \bar{\rho}^{(0.36)} \cdot \bar{I}^{(1.6)}. \tag{14}$$

The energy dissipation for all 16 configurations as a function of impulse ($\bar{I}$) and relative density ($\bar{\rho}$) is shown in Figure 16. Comparing Figure 16 and Figure 12 indicates that the

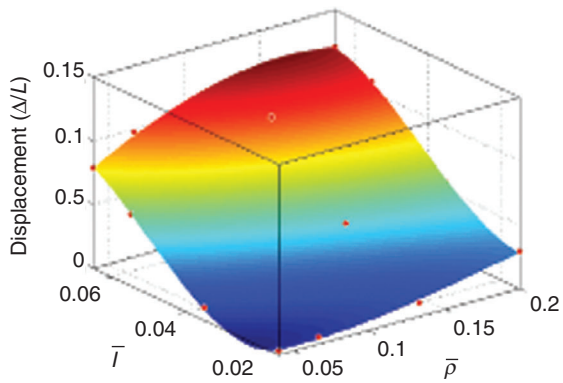


Figure 15 Normalized displacement in water-backed structures as a function of incident impulse $\bar{I}$ and core relative density $\bar{\rho}$.

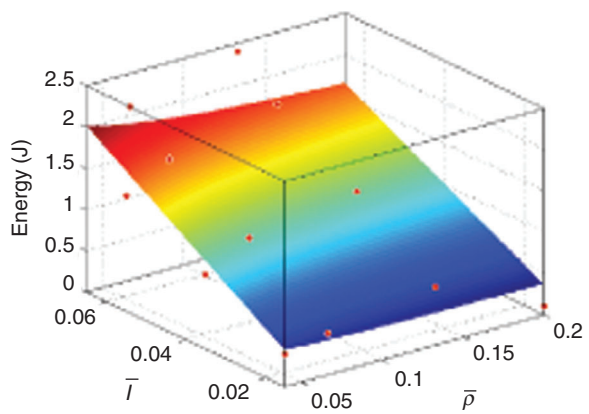


Figure 16 Energy dissipated due to inelastic deformation in water-backed structures as a function of incident impulse $\bar{I}$ and core relative density $\bar{\rho}$.

trend in energy dissipation for the water-backed cases is opposite to that for the air-backed cases. Specifically, structures with low relative density absorb higher amounts of energy. The variation in energy dissipation in water-backed structures ($E_{WB}$) can be quantified using the non-dimensional measures $\bar{I}$ and $\bar{\rho}$ as,

$$E_{WB} = 74.48 \cdot \bar{\rho}^{(-0.12)} \cdot \bar{I}^{(1.02)}. \tag{15}$$

The resistance of a water-backed structure to applied impulse can be quantified by the magnitude of the impulse transmitted into the back-side water. Figure 17 shows the histories of transmitted pressure for different composite structures subjected to identical impulsive loads. The monolithic composite exhibits the least blast mitigation and transmits ~80% of the incident impulse into the back-side water-section. The HP200 core transmits ~40% of

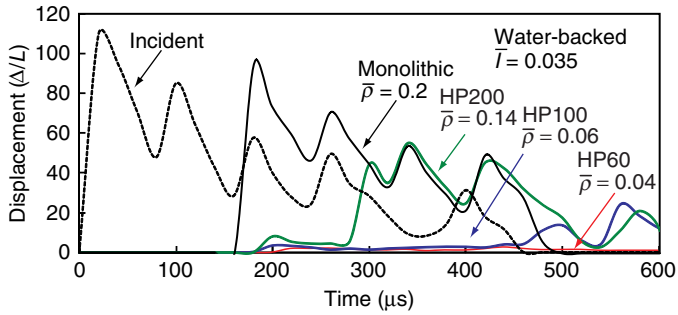


Figure 17 Transmitted pressure as a function of time for monolithic composite and structures with HP60, HP100 and HP200 cores subjected to $\bar{I}$ = 0.035.

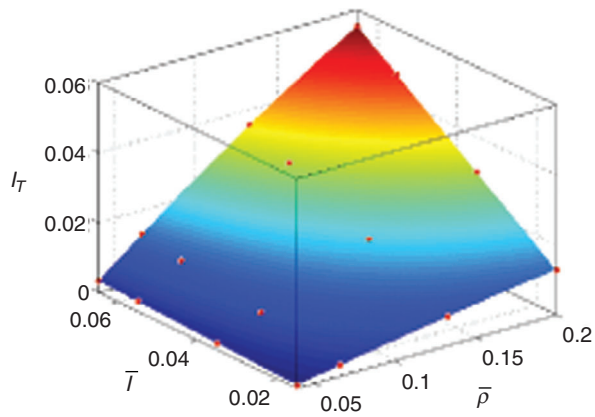


Figure 18 Transmitted impulses measured in the back side water for water-backed structures as a function of incident impulse $\bar{I}$ and core relative density $\bar{\rho}$.

the incident impulse. In the core-compression stage, or at approximately 100 μs, the impulse transmitted is very low. However, when the core fails completely, the front face and the back face move together, causing a pressure wave to be transmitted to the back-side water. The structure with the HP100 core transmits ~20% of the incident impulse with a low-pressure plateau followed by complete core failure and a rise in pressure magnitude. The structure with the HP60 core exhibits superior blast mitigation in comparison to all other structures – transmitting less than 5% of the incident impulse at the end of 1000 μs. Clearly, blast mitigation is relatively insensitive to face thickness and is highly dependent on core-density.

The impulse transmitted by all 16 configurations in the water-backed case is shown as a function of $\bar{I}$ and $\bar{\rho}$ in Figure 18. At all impulse magnitudes, the magnitude of the transmitted impulse increases monotonically with the relative density. The relationship between transmitted impulse ($\bar{I}_T$) and $\bar{I}$ and $\bar{\rho}$ is given by

$$\bar{I}_T = 7.40 \cdot \bar{\rho}^{(1.33)} \cdot \bar{I}^{(1.01)}. \tag{16}$$

## 5.5. STRUCTURAL DESIGN

The preceding discussions have focused on the deformation, deflection and of energy dissipation in composite structures subjected to underwater impulsive loads. In particular, the results of parametric studies have been presented in a format wherein the response variables are functions of the loading (impulse magnitude) and structural attributes (relative density). In structural design, the necessary performance objectives are specified and the structural attributes that fulfill these objectives are identified. Figures 9, 12, 15, 16 and 18 show the effect of loading and structural attributes on dynamic response and give material-structure-performance relationships which are summarized in Table 5. It should be noted that deflection and energy dissipation constitute competing performance requirements. An optimal composite structure design needs to balance low deflection and high energy dissipation. This balance is application-specific and may not be universal. The relations developed in this study allow the identification of optimal structural designs for given combination of deflection, energy dissipation and impulse transmission requirements. For a fixed value of deflection or energy dissipation, the optimum value of relative density for a specific impulsive load can be achieved by varying the material properties of the monolithic plate or sandwich core.

The material-structure-performance relations can be used to inform naval structural design with the precaution that they should only be used for the material, structural parameter ranges and loading conditions considered. Additionally, this study is concerned with the dynamic response of composite structures of equivalent mass. This necessitates significant variations in structural thickness to account for changes in relative densities, which is an important geometric consideration in naval structural design. As the relative density of the structure increases, structural thickness decreases significantly. Structures with high relative densities exhibit higher energy dissipation per unit volume. This aspect is not investigated in the current analysis.

Table 4 Experimental test matrix. The thickness of the facesheets is varied to maintain identical areal mass.

| **Beam Designation** | **Core Density (kg/m$^2$)** | **Core Thickness (mm)** | **Facesheet Thickness (mm)** | **Areal Mass (kg/m$^2$)** |
|---|---|---|---|---|
| M - 1, 2, 3, 4 | — | — | 5 | 10.5 |
| HP60 - 1, 2, 3, 4 | 60 | 30 | 3 | 10.2 |
| HP100 - 1, 2, 3, 4 | 100 | 20 | 3 | 10.4 |
| HP200 - 1, 2, 3, 4 | 200 | 10 | 3 | 10.4 |

Table 5 Summary of material-structure-property relationships.

| | **Air-backed** | **Water-backed** |
|---|---|---|
| Deflection | $\Delta/L_{AB} = 16.54 \cdot \bar{\rho}^{(0.45)}.\bar{I}^{(1.28)}$ | $\Delta/L_{WB} = 19.43 \cdot \bar{\rho}^{(0.36)}.\bar{I}^{(1.6)}$ |
| Energy dissipation | $E_{AB} = 657 \cdot \bar{\rho}^{(0.38)}.\bar{I}^{(1.01)}$ | $E_{WB} = 74.48 \cdot \bar{\rho}^{(-0.12)}.\bar{I}^{(1.02)}$ |
| Impulse transmission | – | $\bar{I}_T = 7.40 \cdot \bar{\rho}^{(1.33)}.\bar{I}^{(1.01)}$ |

## 6. CONCLUSIONS

A marine structure must balance strength and load carrying capacity with the ability to dissipate energy for blast and impact resistance. Composite structures have higher stiffnesses and strength-to-weight ratios than other monolithic structures. Additionally, sandwich structures provide very high bending and shear resistances with slight increases in total mass. However, due to the novelty and wide range of structural combinations, the relationships between dynamic response and material heterogeneity in sandwich structures are not well-quantified. In particular, the behavior of composite structures under extreme impulsive loading generated by underwater explosions needs to be systematically analyzed. In an effort to provide useful information for structural design, the load-carrying capacity and energy-dissipation capabilities of sandwich composites are evaluated over a range of relative densities and impulsive load intensities. The loading conditions involve impulsive loads with peak pressures up to 200 MPa, which simulate the effects of 1 kg of TNT exploding underwater at different stand-off distances from the structure. The constitutive and damage models capture the different inelastic deformations and failure mechanisms in composite laminates and sandwich cores. The findings of this study are as follows.

Comparison of experiments and simulations shows that numerical calculations capture the different damage and dissipation mechanisms in the faces and core. The deformation in sandwich structures is strongly influenced by relative density. Structures with high relative densities undergo severe damage and exhibit significantly higher core face debonding than structures with low relative densities.

For a given impulsive load, structures with low relative densities (HP60 and HP100) experience up to 60% lower displacements than those with high relative densities (HP200 and monolithic). This can be attributed to the higher capacity for core compression and effective load spreading in sandwich cores with low relative density. The relative density has a significant influence on the overall energy dissipation. This is likely due to the fact that low density cores acquire less kinetic energy and enable load spreading. Composite laminates dissipate energy primarily through damage and fragmentation. In sandwich cores, ~98% of total energy dissipation occurs through inelastic deformation and core compression. Although cracking and fragmentation reduces the energy dissipated due to inelastic deformation, these mechanisms only dissipate ~2% of the energy imparted to the sandwich core. The amount of energy dissipated due to damage is significantly higher for structures with high relative densities. Efforts to increase energy absorbency in sandwich structures should focus on multilayered sandwich cores consisting of a combination of materials with low as well as high relative densities.

The presence of water on both sides causes much higher core compression and restricts flexural deformation. The backface deflection is 60% lower and backface velocity is 50% lower in water-backed structures compared with those in air-backed structures.

Based on parametric calculations, material-structure-performance relations are obtained for deflection, energy dissipation, load transmission in terms of incident impulse and relative density. The insight gained here provides guidelines for the design of structures for which response to water-based impulsive loading is an important consideration. Finally, it is instructive to note that the relations described in this paper are applicable only for the structural attributes and loading conditions considered.

## ACKNOWLEDGEMENT

The authors gratefully acknowledge support by the Office of Naval Research through grant numbers N00014-09-1-0808 and N00014-09-1-0618 (program manager: Dr. Yapa D. S. Rajapakse). Calculations are carried out on the Athena HPC cluster in the Dynamic Properties Research Laboratory at Georgia Tech. MZ also acknowledges support from the National Research Foundation of Korea through WCU Grant No. R31-2009-000-10083-0.

## REFERENCES

[1] Abrate, S., *Impact on laminated composite materials*. Appl. Mech. Rev. 44 (4), 155–190., 1991.

[2] Abrate, S., *Impact on laminated composites: recent advances*. Appl. Mech. Rev. 47, 517–544, 1994.

[3] Joshi, S.P. and C.T. Sun, *Impact Induced Fracture in a Laminated Composite*. Journal of Composite Materials, 1985. **19**(1): p. 51–66.

[4] Cantwell, W.J. and J. Morton, *The Impact Resistance of Composite-Materials - a Review.* Composites, 1991. **22**(5): p. 347–362.

[5] Hashin, Z., *Analysis of Stiffness Reduction of Cracked Cross-Ply Laminates*. Engineering Fracture Mechanics, 1986. **25**(5–6): p. 771–778.

[6] Hashin, Z., *Analysis of Orthogonally Cracked Laminates under Tension*. Journal of Applied Mechanics-Transactions of the Asme, 1987. **54**(4): p. 872–879.

[7] Chang, F.K., H.Y. Choi, and S.T. Jeng, *Study on Impact Damage in Laminated Composites*. Mechanics of Materials, 1990. **10**(1-2): p. 83–95.

[8] Chang, F.K., H.Y. Choi, and S.T. Jeng, *Characterization of Impact Damage in Laminated Composites*. Sampe Journal, 1990. **26**(1): p. 18–25.

[9] Lessard, L.B. and F.K. Chang, *Damage Tolerance of Laminated Composites Containing an Open Hole and Subjected to Compressive Loadings .2. Experiment*. Journal of Composite Materials, 1991. **25**(1): p. 44–64.

[10] Minnaar, K. and M. Zhou, *A novel technique for time-resolved detection and tracking of interfacial and matrix fracture in layered materials*. Journal of the Mechanics and Physics of Solids, 2004. **52**(12): p. 2771–2799.

[11] Hashin, Z., *Failure Criteria for Unidirectional Fiber Composites*. Journal of Applied Mechanics-Transactions of the Asme, 1980. **47**(2): p. 329–334.

[12] Fatt, M.S.H. and L. Palla, *Analytical Modeling of Composite Sandwich Panels under Blast Loads*. Journal of Sandwich Structures & Materials, 2009. **11**(4): p. 357–380.

[13] Zenkert, D., *An introduction to sandwich construction*. . Engineering Materials Advisory Service, 1995.

[14] Plantema, F., *Sandwich construction*. New York: Wiley, 1996.

[15] Allen, H., *Analysis and design of structural sandwich panels*. . Oxford: Pergamon Press, 1969.

[16] Steeves, C.A. and N.A. Fleck, *Collapse mechanisms of sandwich beams with composite faces and a foam core, loaded in three-point bending. Part II: experimental investigation and numerical modelling*. International Journal of Mechanical Sciences, 2004. **46**(4): p. 585–608.

[17] Tagarielli, V.L., V.S. Deshpande, and N.A. Fleck, *The dynamic response of composite sandwich beams to transverse impact*. International Journal of Solids and Structures, 2007. **44**(7–8): p. 2442–2457.

[18] Schubel, P.M., J.J. Luo, and I.M. Daniel, *Impact and post impact behavior of composite sandwich panels*. Composites Part a-Applied Science and Manufacturing, 2007. **38**(3): p. 1051–1057.

[19] Nemes, J.A. and K.E. Simmonds, *Low-Velocity Impact Response of Foam-Core Sandwich Composites*. Journal of Composite Materials, 1992. **26**(4): p. 500–519.

[20] Mines, R.A.W., C.M. Worrall, and A.G. Gibson, *The Static and Impact Behavior of Polymer Composite Sandwich Beams*. Composites, 1994. **25**(2): p. 95–110.

[21] J. L. Abot, I.M.D., *Composite sandwich beams under low velocity impact*. Proc. of AIAA Conf. , Seattle, 2001.

[22] Schubel, P.M., J.J. Luo, and I.M. Daniel, *Low velocity impact behavior of composite sandwich panels*. Composites Part a-Applied Science and Manufacturing, 2005. **36**(10): p. 1389–1396.

[23] Tekalur, S.A., A.E. Bogdanovich, and A. Shukla, *Shock loading response of sandwich panels with 3-D woven E-glass composite skins and stitched foam core*. Composites Science and Technology, 2009. **69**(6): p. 736–753.

[24] Espinosa, H.D., S. Lee, and N. Moldovan, *A novel fluid structure interaction experiment to investigate deformation of structural elements subjected to impulsive loading*. Experimental Mechanics, 2006. **46**(6): p. 805–824.

[25] Horacio D. Espinosa , D.G., Félix Latourte and Ravi S. Bellur-Ramaswamy *Failure Modes in Solid and Sandwich Composite Panels Subjected to Underwater Impulsive Loads*. 9th International Conference on Sandwich Structures, ICSS9, 2010.

[26] Wei, Z., et al., *Analysis and interpretation of a test for characterizing the response of sandwich panels to water blast*. International Journal of Impact Engineering, 2007. **34**(10): p. 1602–1618.

[27] LeBlanc, J. and A. Shukla, *Dynamic response and damage evolution in composite materials subjected to underwater explosive loading: An experimental and computational study.* Composite Structures, 2010. **92**(10): p. 2421–2430.

[28] Arora, H., Hooper, P. and Dear, J.P., *Blast and other high rate loading composite sandwich materials*. 9th International Conf on Sandwich Structures (ICSS-9), Ravichandran, G. ed, California Institute of Technology, Pasedena, USA (June 2010), Key-note paper MA3.1., 2010.

[29] Avachat, S. and M. Zhou, *Dynamic Response Of Composite Sandwich Structures Subjected To Underwater Impulsive Loads: Experiments And Simulations* Conference Proceedings of the 16th International Conference on Composite Structures, ICCS-16, A. J. M. Ferreira (Editor), FEUP, Porto, 2011, 2011.

[30] Avachat, S. and M. Zhou, *Dynamic Response of Submerged Composite Sandwich Structures to Blast Loading*. Proceedings of the IMPLAST 2010 - SEM Fall Conference, October 12-14 2010 Providence, Rhode Island, USA, Arun Shukla (Editor), 2010.

[31] Avachat, S. and M. Zhou, *Effect of Facesheet Thickness on Dynamic Response of Composite Sandwich Plates to Underwater Impulsive Loading*. Experimental Mechanics, 2011. **Volume 52**(Issue 1): p. pp 83–93.

[32] Taylor, G.I., *The Scientific Papers of G I Taylor.* Cambridge University Press, Cambridge, 1963.

[33] Cole, R.H., *Spherical Shock Waves from Underwater Explosions*. Physical Review, 1947. **72**(2): p. 177–177.

[34] Kambouchev, N., L. Noels, and R. Radovitzky, *Numerical simulation of the fluid-structure interaction between air blast waves and free-standing plates*. Computers & Structures, 2007. **85**(11–14): p. 923–931.

[35] DIAB Inc., S.D., DeSoto, Texas 75115, USA http://www.diabgroup.com/europe/literature/e_pdf_files/man_pdf/H_man.pdf Accessed 5 May 2011.

[36] Camanho, P.P., C.G. Davila, and M.F. de Moura, *Numerical simulation of mixed-mode progressive delamination in composite materials*. Journal of Composite Materials, 2003. **37**(16): p. 1415–1438.

[37] Hibbit, Karlsson, and Sorensen, *Abaqus/Explicit User's Manual, Version 6.9*. 2009.

[38] Deshpande, V.S. and N.A. Fleck, *Isotropic constitutive models for metallic foams*. Journal of the Mechanics and Physics of Solids, 2000. **48**(6–7): p. 1253–1283.

[39] Deshpande, V.S. and N.A. Fleck, *High strain rate compressive behaviour of aluminium alloy foams*. International Journal of Impact Engineering, 2000. **24**(3): p. 277–298.

[40] Tagarielli, V.L., V.S. Deshpande, and N.A. Fleck, *The high strain rate response of PVC foams and end-grain balsa wood*. Composites Part B-Engineering, 2008. **39**(1): p. 83–91.

[41] Hooputra, H., et al., *A comprehensive failure model for crashworthiness simulation of aluminium extrusions*. International Journal of Crashworthiness, 2004. **9**(5): p. 449–463.

[42] Puck, A. and H. Schürmann, *Failure analysis of FRP laminates by means of physically based phenomenological models*. Composites Science and Technology, Volume 62, Issues 12–13, September–October 2002, Pages 1633–1662, 1999.

[43] Kiel, A.H., *The Response of Ships to Underwater Explosions*. Department of the Navy, 1961.